NIH Public Access
Author Manuscript
Cell. Author manuscript; available in PMC 2012 February 4.

Published in final edited form as:
Cell. 2011 February 4; 144(3): 402–413. doi:10.1016/j.cell.2010.12.031.

Cells Respond to Mechanical Stress by Rapid Disassembly of Caveolae

Bidisha Sinha[1,2,14], **Darius Köster**[1,2,14], **Richard Ruez**[3,4], **Pauline Gonnord**[3,4], **Michele Bastiani**[8,9], **Daniel Abankwa**[8,9], **Radu. V. Stan**[10], **Gillian Butler-Browne**[11], **Benoit Vedie**[12], **Ludger Johannes**[3,4], **Nobuhiro Morone**[13], **Robert G. Parton**[8,9], **Graça Raposo**[3,5,6], **Pierre Sens**[7], **Christophe Lamaze**[3,4,*], and **Pierre Nassoy**[1,2,*]

[1] Université P. et M. Curie/CNRS UMR168, Centre de Recherche, Laboratoire Physico-Chimie, 26 rue d'Ulm, 75248 Paris Cedex 05, France

[2] Institut Curie, Centre de Recherche, Laboratoire Physico-Chimie, 26 rue d'Ulm, 75248 Paris Cedex 05, France

[3] CNRS UMR144, Centre de Recherche, Laboratoire Trafic, Signalisation et Ciblage Intracellulaires, 26 rue d'Ulm, 75248 Paris Cedex 05, France

[4] Institut Curie, Centre de Recherche, Laboratoire Trafic, Signalisation et Ciblage Intracellulaires, 26 rue d'Ulm, 75248 Paris Cedex 05, France

[5] PICT IBiSA Institut Curie, Laboratoire Structure et Compartiments Membranaires, Institut Curie, 26 rue d'Ulm, 75248 Paris Cedex 05, France

[6] Centre de Recherche, Laboratoire Structure et Compartiments Membranaires, Institut Curie, 26 rue d'Ulm, 75248 Paris Cedex 05, France

[7] ESPCI, CNRS-UMR 7083 - Physico-Chimie Théorique, 10 rue Vauquelin, 75231 Paris Cedex 05, France

[8] The University of Queensland, Institute for Molecular Bioscience, Brisbane, Queensland 4072, Australia

[9] Center for Microscopy and Microanalysis, Brisbane, Queensland 4072, Australia

[10] Dartmouth Medical School, Borwell 502W, HB7600, One Medical Center Drive, 03756 Lebanon, NH, USA

[11] Institut de Myologie – Hôpital Pitié-Salpétrière, UM76 UPMC, U974 Inserm, UMR7215 - CNRS-AIM, 47, bld de l'hôpital, 75651 Paris cedex 13, France

[12] Laboratoire de Biochimie, Hôpital Européen Georges Pompidou, 20 rue Leblanc, 75015 Paris, France

[13] National Center of Neurology and Psychiatry, National Institute of Neuroscience, Department of Ultrastructural Research, 4-1-1 Ogawa-Higashi, Kodaira, Tokyo 187-8502, Japan

SUMMARY

[*]Contributed equally and co-corresponding authors: christophe.lamaze@curie.fr, pierre.nassoy@curie.fr.
[14]Contributed equally

Publisher's Disclaimer: This is a PDF file of an unedited manuscript that has been accepted for publication. As a service to our customers we are providing this early version of the manuscript. The manuscript will undergo copyediting, typesetting, and review of the resulting proof before it is published in its final citable form. Please note that during the production process errors may be discovered which could affect the content, and all legal disclaimers that apply to the journal pertain.

NIH-PA Author Manuscript
NIH-PA Author Manuscript
NIH-PA Author Manuscript

NIH-PA Author Manuscript

NIH-PA Author Manuscript

NIH-PA Author Manuscript

The precise role of caveolae, the characteristic plasma membrane invaginations present in many cells, still remains debated. The high density of caveolae in cells experiencing mechanical stress led us to investigate their role in membrane-mediated mechanical response. Acute mechanical stress induced by cell osmotic swelling or by uniaxial stretching results in the immediate disappearance of caveolae, which is associated with a reduced caveolin/Cavin1 interaction, and an increase of free caveolins at the plasma membrane. Tether pulling force measurements in live cells and in plasma membrane spheres demonstrate that caveola flattening and disassembly is the primary actin and ATP-independent cell response which buffers membrane tension surges during mechanical stress. Conversely, stress release leads to complete caveola reassembly in an actin and ATP-dependent process. The absence of a functional caveola reservoir in myotubes from muscular dystrophic patients enhanced membrane fragility under mechanical stress. Our findings support a new role for caveolae as a physiological membrane reservoir that allows cells to quickly accommodate sudden and acute mechanical stresses.

Introduction

Caveolae were first described in the early 1950s through the seminal electron microscopy studies of Palade and Yamada (Palade, 1953; Yamada, 1955). These characteristic 60–80 nm cup-shaped uncoated invaginations are highly enriched in cholesterol and sphingolipids (Richter et al., 2008). Present at the plasma membrane of many cells with the exception of neurons and lymphocytes, they are particularly abundant in muscle cells, adipocytes and endothelial cells. The identification of caveolin-1 (Cav1) (Rothberg et al., 1992; Kurzchalia et al, 1992) and caveolin-2 (Scherer et al., 1996) as the main constituents of the caveolar structure was instrumental to gain insight into the cell biology, structural and genetic features of caveolae (Stan, 2005). They have been associated with endocytosis, cell signaling, lipid metabolism and other functions in physiological as well as in pathological conditions. Nevertheless, the role of these specialized membrane domains remains debated and little is known about the molecular mechanisms involved in their formation and proposed functions (Parton and Simons, 2007).

Recent studies have suggested that the distribution of Cav1, and caveolae-mediated signaling can be affected by external mechanical cues. In endothelial cells, chronic shear exposure activates the ERK pathway in a caveolae-dependent manner (Boyd et al., 2003; Park et al., 2000; Rizzo et al., 2003). In smooth-muscle cells, cyclic stretch can cause association of some kinases with Cav1 (Sedding et al., 2005). To date, the role of Cav1/caveolae in mechanotransduction is mainly viewed as a downstream signaling platform while their function in primary mechanosensing has not been directly addressed. A recent theoretical study has proposed that budded membrane domains like caveolae could play the role of membrane-mediated sensors and regulators of the plasma membrane tension (Sens and Turner, 2006). Endowed with a high membrane and lipid storage capacity, owing to the invaginated structure and high lipid packing, caveolae are well equipped to play such a role.

We have challenged the homeostasis of the plasma membrane tension with different types of controlled mechanical stresses and analyzed the role of caveolae in the cell short-term response. We show in endothelial cells and muscle cells that functional caveolae are required to buffer the variations of membrane tension induced by sudden and transient mechanical stress via a two-step process of rapid caveola disassembly and slower reassembly.

NIH-PA Author Manuscript

NIH-PA Author Manuscript

NIH-PA Author Manuscript

RESULTS

Mechanical Stress Leads to the Partial Disappearance of Caveolae from the Plasma Membrane

We examined the response of caveolae when cells were exposed to acute mechanical stresses. Osmotic swelling causes an increase of the membrane tension of cells unless some additional membrane is delivered to the cell surface (Dai and Sheetz, 1995; Dai et al., 1998; Morris and Homann, 2001). Cav1-EGFP transfected HeLa cells were exposed to hypo-osmotic medium (30m Osm). We observed a 35% increase of the cell volume within the first 5 min and a slow decrease thereafter (Figure 1A and 1B). On reversing back to iso-osmolarity (300 mOsm) after 30 min of hypotonic shock, the volume decreased below the initial cell volume. These observations support the existence of a compensatory mechanism known as regulatory volume decrease, which restores the osmotic balance by activating ions channels (D'Alessandro et al., 2002). Our data however suggest that this process is not dominant during the first 5 minutes following hypo-osmotic shock. To distinguish caveolae at the plasma membrane from the internal Golgi pool of Cav1, we used Total Internal Reflection Fluorescence (TIRF) microscopy (Figures 1C, S1A and S1B). Upon hypo-osmotic shock, we observed that the number of caveolae significantly decreased by ~ 30% at the cell surface (Figures 1C and 1D) and that the loss correlated with the magnitude of the shock (Figure 1E). Importantly, the cell footprint and the adhesion between the cell and the glass surface were unaltered, as shown by Reflection Interference Contrast Microscopy (RICM) (Figure S1C). Since caveolae exhibit different types of dynamics at the plasma membrane (Pelkmans and Zerial, 2005), we also checked whether any particular pool was selectively affected. Within minutes of hypo-osmotic shock, slow moving caveolae reduced their mobility (Figure S1D), fast dynamics were abolished (Supplementary Movies S1A and S1B) while caveolae displaying all kinds of mobility were reduced in number (Figures S1E and S1F). Similar results were obtained in mouse lung endothelial cells (MLEC) (Figure S1B). Although osmotic shocks have been extensively used to mimic the osmolarity changes that cells experience (Lang et al., 1998), we sought to rule out any indirect influence of cell swelling on caveolae. We developed a stretching device based on thin transparent silicone substrates to challenge the cell membrane with a different mechanical stress. It allowed imaging of caveolae by TIRF before and after stretch, and was combined with micropatterning (Chen et al., 1997) to control the cell adhesion area and its orientation with the stretching axis. The number of caveolae present at the basal footprint of Cav1-EGFP HeLa cells decreased upon stretching (Figures 1F and 1G), and the loss correlated with the extent of stretch (Figure 1H). Therefore, acute mechanical stress induced either by hypo-osmotic shock or membrane stretching, leads to a rapid and significant loss of caveolae from the cell surface. We next performed electron microscopy (EM) on MLEC. These endothelial cells experience chronic cycles of shear stress from the blood flow in lungs' vessels *in vivo*. MLEC immunostaining shows multiple subcellular Cav1 positive structures, which are localized predominantly at the plasma membrane and at the Golgi apparatus (Figure S3B; Murata et al., 2007). In contrast, $Cav1^{-/-}$ MLEC derived from cells knocked out for the CAV1 gene do not present any Cav1 staining. However, Cav1-EGFP expression can be induced by transfection in wt and $Cav1^{-/-}$ MLEC (Figure S3C). EM analysis showed a significant decrease of the number of caveolae (50%) upon a 5 min exposure of wt MLEC to a hypo-osmotic shock (Figures 2A and 2B). These data confirm the results obtained by TIRF imaging, and extend our conclusions to endogenous caveolae present on the entire surface of the cell.

Flattening and Disassembly of Caveolae on Hypo-Osmotic Shock

The contribution of caveolae to the general endocytic activity of the cell is believed to be minimal (Nabi and Le, 2003), and endocytosis is disfavored at high membrane tension (Dai

NIH-PA Author Manuscript

NIH-PA Author Manuscript

NIH-PA Author Manuscript

et al., 1997). We still tested if the loss of caveolae upon hypo-osmotic was due to increased caveola endocytosis. We used dynasore, an inhibitor of the dynamin GTPase which is involved in caveola internalization (Henley et al., 1998; Macia et al., 2006). Indeed, dynasore significantly increased the caveolae density at the plasma membrane reflecting the efficient inhibition of caveola endocytosis (Figure 2C). However, upon hypo-osmotic shock, a similar loss of caveolae was measured (Figures 2C and 2D). We next examined Cavin1, which is part of the caveolar complex and required to maintain caveola invagination (Hill et al., 2008, Hansen et al., 2009). Cavin1 does not bind to free Cav1 oligomers or to Cav1 present on the Golgi apparatus. We found a high level (64%) of Cav1-EGFP colocalization with Cavin1-mCherry (Figure 2E). Upon hypo-osmotic shock, there was a similar or even higher loss of Cavin1 labeled structures confirming the partial loss of caveolae (Figure 2F). We also observed a decreased colocalization with Cavin1 (35%) for the remaining caveolae, suggesting a loss of their invaginated structure. We quantified the interaction between Cav1 and Cavin1 using fluorescence lifetime imaging microscopy (FLIM). When Cavin1 is present in caveola, the close proximity of mRFP-Cav3 and Cavin1-EGFP results in FRET and a decrease in the EGFP fluorescence lifetime (Abankwa et al., 2008; Hill et al., 2008). There was a significant increase in the fluorescence lifetime on hypo-osmotic shock, indicating the dissociation of Cavin1 from Cav1 (Figure 2G). We also performed Cav1 immuno-EM on MLEC before and after hypo-osmotic shock (Figure 3A and S2A). We found a ten-fold increase in the number of gold particles associated with Cav1 in non-caveolar membranes after 5 min of hypo-osmotic shock (Figure 3B). On returning to iso-osmolarity, cells recovered the initial number of caveolae, and Cav1 was mainly associated with caveola (Figures 3B and 3C). Under iso-osmotic conditions, deep-etched EM showed a majority of budded caveolae with characteristic tight striated-coats (Morone et al., 2006). After hypo-osmotic shock, several flat structures with loose striated-coats reminiscent of formerly budded caveolae were observed. Upon iso-osmolarity recovery, all caveolae were budded (Figures 3D, and S2B for 3D view). These findings clearly indicate that cells respond to acute mechanical membrane stress by the rapid flattening of a fraction of the caveola. We also measured the level of Cav1-EGFP diffusing freely at the membrane using fluorescence recovery after photobleaching (FRAP). At steady state, the fraction of freely diffusing Cav1 in the plasma membrane was low (10%; Figure 3E), as reported (Pelkmans et al., 2004; Hill et al, 2008). However, we measured a higher mobile fraction (30%) in cells exposed to hypo-osmotic shock for at least 10 min. This increase is likely to reflect the release of Cav1 from flattened caveolae.

Caveolae are Selectively Required for Buffering Membrane Tension

Caveola flattening is likely to release the amount of membrane stored within the caveolar invagination, and thereby to provide the additional membrane required to maintain membrane tension homeostasis during mechanical stress (Sens and Turner, 2006). We tested this hypothesis with the tether pulling technique (Dai and Sheetz, 1995), which measures the cell membrane tension. Optically trapped beads adhering to the plasma membrane served as handles to extract membrane tethers (Figures 4A and S3A, and Supplementary Movie S2). The restoring tether force *f*, which was derived from the bead displacement, is an indicator of the effective membrane tension (Sheetz, 2001). Its value is proportional to the square root of the effective tension $\tilde{\sigma}$, which corresponds to the sum of the lipid bilayer tension σ and the cytoskeleton-to-membrane adhesion energy W_0. The latter term represents ~ 75% of $\tilde{\sigma}$ (Dai and Sheetz, 1999) and arises from all molecular interactions between membrane and cytoskeleton. The presence of exogenous proteins is thus likely to have an intricate influence on W_0, as shown later. Tether force measurements do not enable *a priori* to separate σ and W_0. Therefore, we used the tether pulling technique as a differential assay to probe the relative changes in tether forces under conditions that keep W_0 unaltered. In particular, osmotic shocks have been assumed to mostly impact on σ with minor changes on adhesion

NIH-PA Author Manuscript

NIH-PA Author Manuscript

NIH-PA Author Manuscript

(Dai et al., 1998). By quantifying the actin bundles architecture, we found that the cortical actin cytoskeleton was unaltered within the first 5 minutes of osmotic shock (Figures S3D–F). At these timescales, variations in f thus directly mirror changes in σ. We measured the tether force f_0 in isotonic conditions and recorded the variations of the tether force f while MLEC were exposed to hypo-osmotic shock. Figure 4A shows representative temporal traces of the relative tether force changes, $(f-f_0)/f_0$, obtained in wt and Cav1$^{-/-}$ MLEC. We found that upon hypo-osmotic shock (150 mOsm), f remained almost identical to f_0 in wt MLEC. In contrast, the tether force increased by 200% in Cav1$^{-/-}$ MLEC. Our data imply that the membrane tension increase is buffered in wt MLEC by the presence of caveolae. Importantly, the expression of functional caveolae by transfection of Cav1-EGFP in Cav1$^{-/-}$ MLEC restored membrane tension buffering. Therefore the lack of membrane tension buffering is due to the absence of caveolae and not to other cellular structures that may have been altered in Cav1$^{-/-}$ MLEC (Figure 4A). M-β-cyclodextrin, which flattens caveolae through cholesterol depletion (Rothberg et al., 1992), led also to membrane tension increase upon hypo-osmotic shock in wt MLEC (Figure 4A), confirming that caveola flattening is required for buffering the membrane tension surge. Finally, we have calculated that the number of lost caveolae per cell observed by TIRF and EM is in excellent agreement with the amount of released area (~0.3%) required to buffer σ (see Supplementary Text).

We also tested whether clathrin-coated pits (CCP), another type of plasma membrane invaginations, could buffer membrane tension. Thus, we quantitatively analyzed the fate of CCPs upon hypo-osmotic shock in MLEC and HeLa cells. We observed that the number of CCPs lost at the membrane was at most one tenth of the number of lost caveolae, both in wt and Cav1$^{-/-}$ MLEC (Figures S4A–C). Accordingly, deep-etch EM showed that the structure of CCPs was not affected (Figure 3D). Additionally, under hypo-osmotic shock, membrane tension was buffered to the same extent whether clathrin was expressed or knocked down in wt MLEC (Figures S4D and S4E). In contrast, Cav1$^{-/-}$ MLEC having CCPs could not buffer the membrane tension surge. These results rule out a contribution of CCPs in membrane tension regulation and establish caveolae as the primary stress-responsive membrane structure.

Finally, we obtained similar results in Cav1-EGFP HeLa and in embryonic fibroblasts (MEF) lacking or expressing Cav1 (Figure 4B). We could further extend the physiological significance of these findings by measuring the stress reactivity of human muscle cells. Several human muscular dystrophies have been associated with mutations in Cav3, the muscular isoform of caveolin (Woodman et al., 2004), and more recently with mutations in Cavin1 (Hayashi et al., 2009). Most Cav3 mutations prevent caveolae assembly at the plasma membrane by sequestration of Cav3 in the Golgi apparatus. We studied differentiated human myotubes bearing the P28L Cav3 mutation described in familial hyperCK-aemia (FHCK), a hereditary form of muscular dystrophy (Woodman et al., 2004). Muscle fibers isolated from these patients show a strong decrease of Cav3 expression and reduced Cav3 staining at the cell surface (Merlini et al., 2002). Accordingly, we found that Cav3 immunostaining was restricted to the Golgi apparatus in P28L Cav3 myotubes, whereas wt Cav3 was mainly found at the plasma membrane (Figure 4C). Under hypo-osmotic shock, membrane tension was increased in P28L Cav3 myotubes and buffered in wt Cav3 myotubes (Figure 4D). P28L myotubes and Cav1$^{-/-}$ MLEC showed also an increased tendency to membrane rupture under hypo-osmotic shock (Figure S5). This may explain the high blood level of creatine kinase found in these patients, in the absence of a functional caveolar reservoir during the repeated extension-relaxation cycles.

NIH-PA Author Manuscript

NIH-PA Author Manuscript

NIH-PA Author Manuscript

Membrane Tension Surge Buffering by Caveola Flattening Occurs in an ATP and Actin Independent Process

Although the actin cytoskeleton was unaffected by hypo-osmotic shocks at early times, we still investigated its potential role in caveola flattening. Under hypo-osmotic shock (30 mOsm), none of the actin-perturbing drugs prevented the loss of caveolae from the membrane (Figure 5A). This was further confirmed by cell ATP depletion before hypo-osmotic shock. ATP depletion abolished the mobility of the internal pool of caveolae confirming the inhibition of active cellular processes (Supplementary Movie S3A and S3B). However, a similar loss of caveolae occurred in ATP-depleted cells (Figure 5A). Likewise, upon cell stretching, caveolae still disappeared in ATP-depleted and cytochalasin D (CD) treated cells (Figures 5B and S6A). Furthermore, membrane tension measurements under hypo-osmotic shock (150 mOsm), showed that the tether force of $Cav1^{-/-}$ MLEC still increased by 200% in cells treated with CD or depleted in ATP (Figures 5C and S6B). In contrast, no significant tether force variation was measured for wt MLEC, indicating that the buffering is not dependent on ATP and actin dynamics. Importantly, the invaginated shape of caveola was unaffected by CD or ATP depletion (Figure S7). Finally, we could unambiguously establish that membrane tension buffering is an intrinsic mechanical property of caveolae by using plasma membrane spheres (PMS). PMS are composed of plasma membrane and cytosol while the subcellular compartments (Lingwood et al., 2008) and filamentous actin (Figure S6C) are excluded. PMS were prepared from MLEC transfected with Cav1-EGFP and Cavin1-mCherry. As expected, a major colocalization of Cavin1 and Cav1 was observed at the plasma membrane of the donor cell (Figure 5D). Confocal imaging revealed that Cavin1 was present inside PMS and along the membrane, where it colocalized with Cav1 as a punctuated pattern likely to reflect the incorporation of caveolar invaginations in these vesicles (Figure 5E). PMS were then mechanically stressed by micropipette aspiration (Dimova et al., 2006). Membrane tethers were pulled with optical tweezers from PMS aspirated under minimal pressure (Figure 5E). On increasing aspiration pressure, PMS from $Cav1^{-/-}$ MLEC exhibited a steady tether force increase, whereas *f* remained constant over a significant range of aspiration pressures in PMS from wt MLEC (Figure 5F). Concomitantly, over the aspiration range corresponding to the force plateau, the number of Cavin1/Cav1 colocalizations also decreased to noise level (Figure 5E). When the aspiration was increased further, the force plateau was followed by an increase in *f*, which is in agreement with the complete flattening of caveolae, and thus depletion of all residual membrane reservoir (Figure 5F). We also measured identical amounts of free cholesterol in wt and $Cav1^{-/-}$ PMS (~75 ± 20 nmol/mg of cell protein), indicating that the lack of buffering effect in $Cav1^{-/-}$ PMS is not related to changes in lipid composition. These results on PMS reinforce our findings obtained with actin drugs and ATP depletion in cells, and definitely establish that membrane tension buffering by caveolae flattening is a purely passive mechanism solely driven by membrane mechanics.

Caveolae Reassemble in an Actin and ATP Dependent Process upon Stress Relaxation

We next examined the behavior of caveolae when cells were left in hypo-osmotic medium (30 mOsm) for 5 min and returned to iso-osmotic medium (300 mOsm). Within 2–5 min, caveolae re-appeared at the plasma membrane (Figures 3A, 3B, 3C, 3D and 6A). Accordingly, there was a decrease of both the fraction of mobile Cav1 (Figure 3E) and Cav1 immuno gold labeling in non-caveolar membranes (Figures 3A, 3B and S2A). We also measured a decrease in EGFP fluorescence lifetime indicating the re-association of Cav1 and Cavin1, and therefore the reassembly of functional caveolae at the cell surface (Figure 6B).

On average, the initial rate of reassembly was about 10 caveolae per min per cell, and required ATP (Figure 6C). In contrast to caveolae disassembly, reassembly was enhanced

NIH-PA Author Manuscript

NIH-PA Author Manuscript

NIH-PA Author Manuscript

when actin dynamics were blocked by CD. Finally, we tested whether caveolae reassembled directly from the plasma membrane pool of free Cav1 or from other compartments. The disruption of the Golgi apparatus by Brefeldin A (BFA) did not prevent reassembly excluding a major contribution of the Cav1 Golgi pool (Figure 6D). Furthermore, we found no significant transfer of the photoconverted Golgi pool of Cav1 to the plasma membrane on returning to iso-osmolarity. However, the non-photoconverted Cav1 present throughout the cell showed an increased punctuated localization at the plasma membrane (Figure 6E and 6F).

DISCUSSION

Since their discovery in 1953, the precise role of caveolae has remained a matter of considerable debate. Freeze-fracture analysis of the surface membrane of smooth and striated muscle cells in the early 1970's led to the first hypothesis that caveolae could flatten out under stretching conditions (Dulhunty and Franzini-Armstrong, 1975; Prescott and Brightman, 1976). Later studies have also associated caveolae with the mechanosensing response of the cell (Boyd et al., 2003; Park et al., 2000; Rizzo et al., 2003; Sedding et al., 2005; Kawamura et al., 2003; Kozera et al., 2009). Whether caveolae are directly involved in the cell response to mechanical stress, and by which mechanisms, still remain unknown. In this study, we establish that the primary cell response to an acute mechanical stress occurs through the rapid flattening of caveolae into the plasma membrane. Upon cell stretching or osmotic swelling, caveolae flattening provides the additional amount of membrane that inhibits any surge of membrane tension. This response occurs also in ATP depleted cells, and in membrane-derived vesicles devoid of actin, indicating that the ability to buffer membrane tension is intrinsic to the caveola structure. These results are in line with a theoretical model proposing that invaginated domains can serve as a membrane reservoir to regulate the membrane tension (Sens and Turner, 2006). However, in contrast to this model, which predicted that flattening of existing caveolae or budding of new caveolae was driven by the deviation of the membrane tension with respect to the resting tension, our data indicate that the regulatory mechanism is asymmetric. While stress-induced flattening of caveolae is truly passive, the reassembly of new caveolae is assisted by ATP and actin dynamics. The energy landscape for flat and invaginated caveola is thus characterized by an activation energy. The transition between the two forms thus requires an energy barrier to be overcome or lowered. In this model, the flat configuration would be stabilized upon application of a mechanical force, whereas the formation of invaginated caveola is energetically favored through interactions with cortical actin in the presence of ATP. This is consistent with the known role of actin dynamics and various kinases in caveola function (Pelkmans et al., 2005; Pelkmans and Zerial, 2005). Our results further indicate that clathrin-coated pits, the other abundant invaginations present at the plasma membrane, are not involved in the fast response to membrane strain. Whereas CCPs exchange coat proteins within seconds, most caveolae are rather stable at the plasma membrane. The stability of caveolae combined with their low endocytic activity allows this membrane reservoir to be readily available to respond to sudden mechanical strains. The stability of the caveolae reservoir is a striking feature of cells that experience pulsating mechanical stresses in their lifetime (muscle cells, cardio-myocytes, endothelial cells), since they all express very high numbers of caveolae. Indeed, we could associate the lack of Cav3 expression at the surface of myotubes with impaired membrane tension buffering in patients bearing the Cav3 P28L mutation found in a form of human muscular dystrophy. Interestingly, P28L myotubes appear to be more fragile than wt myotubes when exposed to acute osmotic shock.

We have shown that the timescales of caveolae and actin cortex responses to osmotic shock are well separated (< 2 min and > 5 min, respectively). While the immediate response to mechanical stress relies primarily on caveola flattening, it is likely that other processes such

NIH-PA Author Manuscript

NIH-PA Author Manuscript

NIH-PA Author Manuscript

as endocytosis, exocytosis and actin dynamics may prolong or complete the initial response at longer times. Whether, and how caveolae also contribute to long timescale regulation remains to be investigated. In endothelial cells, the application of chronic and repetitive shear stress tensions results in a several-fold increase of the number of caveolae at the plasma membrane, through the mobilization of the Cav1 pool associated with the Golgi complex (Boyd et al., 2003; Park et al., 1998). In agreement with the slow delivery rate of Cav1 from the Golgi complex (Tagawa et al., 2005), we show that caveolae are reassembled independently from the Golgi complex when the mechanical stress is relaxed. It is thus important to distinguish between the short-term mechanical function of caveolae and the long-term adaptation of the cell to chronic stress. In this context, we also analyzed the contribution of caveolae to the setting of the membrane tension under resting conditions. At steady state, we measured a lower membrane tension in $Cav1^{-/-}$ than in wt MLEC, however it was identical in wt and $Cav1^{-/-}$ MEF, albeit to a lower level (Figure S8A), raising the possibility of a peculiarity of MLEC. Furthermore, the resting tension was drastically affected by m-β-cyclodextrin, cytochalasin D or ATP depletion treatments in the different cell types, independently from the expression of caveolae (Figure S8B). Although caveolae play a key role in cell tension homeostasis, their direct contribution to the resting tension remains intricate. As previously mentioned, the dynamic membrane-to-cytoskeleton adhesion, which is the main contribution to the apparent membrane tension, is likely to be regulated by cell line-dependent compensatory mechanisms.

The well-conserved scaffolding domain of caveolin (CSD) has been involved in both the assembly of caveolae and the interaction with several signaling effectors *in vitro* (Parton et al., 2006; Parton and Simons, 2007). Since several of these effectors have been associated with mechanotransduction (Vogel and Sheetz, 2006), stress-induced disassembly of caveolae may generate mechano-sensitive signals mediating the short and long-term cell response to mechanical challenges. It is tempting to speculate that the mechanical release of free Cav1 oligomers could favor the interaction between signaling effectors and CSD, which is otherwise hidden in the caveolar structure (Kirkham et al., 2008; Parton et al., 2006). This mechano-sensitive signaling would be terminated through the reassembly of free Cav1 oligomers into caveolae when the mechanical stress is relaxed. Endocytosis, which is favored for the retrieval of the excess of membrane during tension relaxation, may also contribute to signaling termination through the internalization of free Cav1 and its degradation in the endolysosomal pathway. The recently characterized Cavin1 protein, which was first described as a transcription factor (Jansa et al., 2001) may also contribute to mechanosignaling regulation through the release from flattened caveola. Indeed, the redistribution of Cav1 to non-caveolar portions of the plasma membrane, the increased mobility of Cav1, and the decreased association of Cav1 and Cavin1 upon hypo-osmotic treatment are all consistent with the effect of Cavin1 knockdown on these parameters (Hill et al., 2008), suggesting that dissociation of the Cav1-cavin module may be crucial in the caveolar response.

Our study establishes a new physiological mechanism by which cells can respond immediately to sudden variations in membrane tension induced by acute mechanical stress (Figure 7). The different proposed roles of caveolae should therefore be reconsidered through this unique ability to respond to mechanical stress, especially in situations where cells experience physiological or pathological membrane strains such as osmotic swelling, shear stress or mechanical stretching.

EXPERIMENTAL PROCEDURES

A list of chemicals and materials can be found in the Extended Experimental Procedures.

NIH-PA Author Manuscript

NIH-PA Author Manuscript

NIH-PA Author Manuscript

Cell culture and Treatments

MLEC (Murata et al., 2007) were maintained in EGM-2/20%FBS medium. They were transfected with AMAXA HUVEC nucleofector kit and used for experiments after 24–72 hrs. HeLa cells stably transfected with Cav1-EGFP (Pinaud et al., 2009) and MEFs were maintained in DMEM/10% FBS. HeLa cells were transfected with FuGENE or Lipofectamine 2000 and used after 16 hrs. Human muscle cells were maintained in X medium (64% DMEM, 16% 199 Medium, 20% FBS, 2,5 ng/ml HGF, 50 μg/ml gentamycin + 10^{-7} M dexamethasone). For differentiation, cells were grown on collagen type I coated surface for 7–10 days in DMEM supplemented with 50 μg/ml gentamycin, 10 μg/ml of bovine insulin and 100 μg/ml of human apotransferrin. For dynasore treatment, cells were washed thrice with PBS^{++} (Phosphate Buffer Saline + 1.5 mM Ca^{++} + 1.5 mM Mg^{++}) and overlaid with 80μM dynasore in PBS^{++}. Cytochalasin D (CD), Latrunculin A (Lat) and Jasplakinolide (Jas) were used for 15 min at 37°C at 5 μg/ml, 1μM or 1μM, respectively in normal medium. ATP depletion was performed by incubating the cells for 30 min at 37°C in PBS^{++} with 10 mM deoxy-D-glucose and 10 mM NaN_3. For disrupting the Golgi apparatus, cells were pretreated for 50 min with 10 μg/ml BFA. Cells were incubated for 50 min in PBS^{++} supplemented with 5 mM mβCD to extract cholesterol. Hypo-osmotic shock was performed on pre-treated cells by using growth medium diluted appropriately in deionized water (1:9 dilution for 30 mOsm hypo-osmotic shock and 1:1 for 150 mOsm hypo-osmotic shock). The concentration of all drugs was maintained during the hypo-osmotic shock as well as during recovery.

Membrane Tether Extraction and Force Measurements

Plasma membrane tethers were pulled out from cells by a concanavalin A-coated bead trapped in optical tweezers (Cuvelier et al., 2005). After extraction, the tether was held at a constant length between 5 and 150 μm, and tether forces were measured from the detected position of the bead after calibration of the optical trap. Samples were maintained at 37°C throughout.

PMS Formation and Micropipette Aspiration

Plasma membrane spheres (PMS) were generated by a protocol adapted from (Lingwood et al., 2008). Cells were grown on glass cover slips and incubated for 6–8 hrs in PBS^{++} supplemented with 10 μM MG132. Individual PMS were selected for micropipette aspiration experiments as described previously for lipid vesicles (Sorre et al., 2009). In brief, PMS were held with a micropipette (diameter ~3 μm) under slight aspiration. By partially entering the pipette, the membrane is strained. Tether forces were measured as explained above while the aspiration of the PMS was gradually increased.

Fluorescence Imaging and Analysis

TIRF microscopy was performed using a 100X, 1.45 NA objective and an EMCCD camera (Hamamatsu Photonics, Japan) in a Zeiss Axiovert 200 microscope. Confocal imaging was performed on a Nikon A1R microscope with a 100X, 1.4 NA objective at 1 airy unit pinhole aperture. TIRF-FRAP experiments (5×5 μm bleaching region) were performed on a Nikon Eclipse 2000 microscope equipped with an EMCCD camera (Roper Scientific, Tucson, AZ). Cells were maintained at 37°C during imaging. Confocal images of PMS were taken in a z-section of width 0.4 μm around the equatorial plane. Image analysis (caveolae detection, volume measurement, FRAP, colocalization) was done using Labview 8.5 and Vision 8.5 (National Instruments, Austin, TX) as detailed in the Extended Experimental Procedures. FLIM microscopy was performed as described previously (Hill et al., 2008).

NIH-PA Author Manuscript

NIH-PA Author Manuscript

NIH-PA Author Manuscript

Cell Stretching

Cells were grown on a rectangular PDMS sheet (thickness ~100 μm, dimensions ~ 12×7 mm) decorated with adhesive micropatterns and stretched uniaxially using a custom-built device equipped with a motorized linear actuator (PI, Karlsruhe, Germany) and a temperature controller. Imaging was done on the TIRF microscope. Strains were applied in ~ 5 sec and the number of caveolae was measured from images taken within 1–3 minutes of stretching.

Immunofluorescence Studies

Cells were fixed, immunolabeled and imaged on an inverted microscope (Leica, Wetzlar, Germany).

Deep-Etched EM of the Cytoplasmic Surface of MLEC

Cells grown on coverslips were prepared by first unroofing their apical surface, and then fixing and freezing the basal surface. The cytoplasmic surface was deeply etched and rotary shadowed with platinum/carbon at an angle of 22°C from the surface and with carbon from the top. The replica was mounted on the sample grid and observed using a transmission electron microscope.

Electron Microscopy

For conventional EM, cells were grown on coverslips, fixed, dehydrated and embedded in epon. For ultrathin cryosectioning and immunogold labeling, cells were fixed and processed for ultracryomicrotomy and immunogold labeled. Quantification of caveolae was done by counting only the number of neck-open caveolae at the plasma membrane in EM images that had at least one caveola.

Supplementary Material

Refer to Web version on PubMed Central for supplementary material.

Acknowledgments

This work was supported by the Institut Curie (PIC Division Cellulaire, Polarité et Cancer), Agence Nationale pour la Recherche, Fondation de France (programme tumeurs), Association Française contre les Myopathies, the National Health and Medical Research Council of Australia and the Australian Research Council (RGP, DA) and NIH grants HL83249 and HL92085 (RVS). Microscopy (MB) was performed at the ACRF/IMB Dynamic Imaging Centre for Cancer Biology. DK was funded by a doctorate fellowship from the Institut Curie and BS was funded by postdoctoral fellowships from the Institut Curie and the Association pour la Recherche sur le Cancer. DA is a fellow of the Swiss National Science Foundation (PA00A-111446) and is indebted to K. Alexandrov for support. The authors gratefully acknowledge the Nikon Imaging Centre at Institut Curie and the CNRS consortium CellTis. We thank F. Perez for the pDendra2-C plasmid, A. Helenius for the Cav1-EGFP plasmid and MEF cells, and F. Pinaud for Cav1-EGFP HeLa. We are also grateful to M. Piel and N. Carpi for help in micropatterning, and P. Bassereau for access to the confocal microscope coupled to optical tweezers. We thank C. Viaris and C. Blouin for carefully reading the manuscript, and we are indebted to A. Bigot for providing human muscle cells. We would like to thank Eurobiobank and Pr. C. Minette for giving access to primary cells to isolate the immortalized Cav3 cell line. C.L. wishes to dedicate this work to the memory of his father, Robert Lamaze, and to all patients suffering from pancreatic cancer.

References

Abankwa D, Hanzal-Bayer M, Ariotti N, Plowman SJ, Gorfe AA, Parton RG, McCammon JA, Hancock JF. A novel switch region regulates H-ras membrane orientation and signal output. EMBO J 2008;27:727–735. [PubMed: 18273062]

NIH-PA Author Manuscript

NIH-PA Author Manuscript

NIH-PA Author Manuscript

Boyd NL, Park H, Yi H, Boo YC, Sorescu GP, Sykes M, Jo H. Chronic shear induces caveolae formation and alters ERK and Akt responses in endothelial cells. Am J Physiol Heart Circ Physiol 2003;285:H1113–1122. [PubMed: 12763750]

Chen CS, Mrksich M, Huang S, Whitesides GM, Ingber DE. Geometric control of cell life and death. Science 1997;276:1425–1428. [PubMed: 9162012]

Cuvelier D, Derenyi I, Bassereau P, Nassoy P. Coalescence of membrane tethers: experiments, theory, and applications. Biophys J 2005;88:2714–2726. [PubMed: 15695629]

Dai J, Sheetz MP. Regulation of endocytosis, exocytosis, and shape by membrane tension. Cold Spring Harb Symp Quant Biol 1995;60:567–571. [PubMed: 8824429]

Dai J, Sheetz MP. Membrane tether formation from blebbing cells. Biophys J 1999;77:3363–3370. [PubMed: 10585959]

Dai J, Sheetz MP, Wan X, Morris CE. Membrane tension in swelling and shrinking molluscan neurons. J Neurosci 1998;18:6681–6692. [PubMed: 9712640]

Dai J, Ting-Beall HP, Sheetz MP. The secretion-coupled endocytosis correlates with membrane tension changes in RBL 2H3 cells. J Gen Physiol 1997;110:1–10. [PubMed: 9234166]

D'Alessandro M, Russell D, Morley SM, Davies AM, Lane EB. Keratin mutations of epidermolysis bullosa simplex alter the kinetics of stress response to osmotic shock. J Cell Sci 2002;115:4341–4351. [PubMed: 12376565]

Dimova R, Aranda S, Bezlyepkina N, Nikolov V, Riske KA, Lipowsky R. J Phys Condens Matter 2006;18:S1151–S1176.

Dulhunty AF, Franzini-Armstrong C. The relative contributions of the folds and caveolae to the surface membrane of frog skeletal muscle fibres at different sarcomere lengths. J Physiol 1975;250:513–539. [PubMed: 1080806]

Hansen CG, Bright NA, Howard G, Nichols BJ. SDPR induces membrane curvature and functions in the formation of caveolae. Nat Cell Biol 2009;11:807–814. [PubMed: 19525939]

Hayashi YK, Matsuda C, Ogawa M, Goto K, Tominaga K, Mitsuhashi S, Park YE, Nonaka I, Hino-Fukuyo N, Haginoya K, et al. Human PTRF mutations cause secondary deficiency of caveolins resulting in muscular dystrophy with generalized lipodystrophy. J Clin Invest 2009;119:2623–2633. [PubMed: 19726876]

Henley JR, Krueger EW, Oswald BJ, McNiven MA. Dynamin-mediated internalization of caveolae. J Cell Biol 1998;141:85–99. [PubMed: 9531550]

Hill MM, Bastiani M, Luetterforst R, Kirkham M, Kirkham A, Nixon SJ, Walser P, Abankwa D, Oorschot VM, Martin S, et al. PTRF-Cavin, a conserved cytoplasmic protein required for caveola formation and function. Cell 2008;132:113–124. [PubMed: 18191225]

Jansa P, Burek C, Sander EE, Grummt I. The transcript release factor PTRF augments ribosomal gene transcription by facilitating reinitiation of RNA polymerase I. Nucleic Acids Res 2001;29:423–429. [PubMed: 11139612]

Kawamura S, Miyamoto S, Brown JH. Initiation and transduction of stretch-induced RhoA and Rac1 activation through caveolae: cytoskeletal regulation of ERK translocation. J Biol Chem 2003;278:31111–31117. [PubMed: 12777392]

Kirkham M, Nixon SJ, Howes MT, Abi-Rached L, Wakeham DE, Hanzal-Bayer M, Ferguson C, Hill MM, Fernandez-Rojo M, Brown DA, et al. Evolutionary analysis and molecular dissection of caveola biogenesis. J Cell Sci 2008;121:2075–2086. [PubMed: 18505796]

Kozera L, White E, Calaghan S. Caveolae act as membrane reserves which limit mechanosensitive $I_{Cl,swell}$ channel activation during swelling in the rat ventricular myocyte. PLoS One 2009;4:e8312. [PubMed: 20011535]

Kurzchalia TV, Dupree P, Parton RG, Kellner R, Virta H, Lehnert M, Simons K. VIP21, a 21-kD membrane protein is an integral component of trans-Golgi-network-derived transport vesicles. J Cell Biol 1992;118:1003–1014. [PubMed: 1512286]

Lang F, Busch GL, Ritter M, Volkl H, Waldegger S, Gulbins E, Haussinger D. Functional significance of cell volume regulatory mechanisms. Physiol Rev 1998;78:247–306. [PubMed: 9457175]

Lingwood D, Ries J, Scwille P, Simons K. Plasma membranes are poised for activation of raft phase coalescence at physiological temperature. Proc Natl Acad Sci USA 2008;105:10005–10010. [PubMed: 18621689]

NIH-PA Author Manuscript

NIH-PA Author Manuscript

NIH-PA Author Manuscript

Macia E, Ehrlich M, Massol R, Boucrot E, Brunner C, Kirchhausen T. Dynasore, a cell-permeable inhibitor of dynamin. Dev Cell 2006;10:839–850. [PubMed: 16740485]

Merlini L, Carbone I, Capanni C, Sabatelli P, Tortorelli S, Sotgia F, Lisanti MP, Bruno C, Minetti C. Familial isolated hyperCKaemia associated with a new mutation in the caveolin-3 (CAV-3) gene. J Neurol Neurosurg Psychiatry 2002;73:65–67. [PubMed: 12082049]

Morone N, Fujiwara T, Murase K, Kasai RS, Ike H, Yuasa S, Usukura J, Kusumi A. Three-dimensional reconstruction of the membrane skeleton at the plasma membrane interface by electron tomography. J Cell Biol 2006;174:851–862. [PubMed: 16954349]

Morris CE, Homann U. Cell surface area regulation and membrane tension. J Membr Biol 2001;179:79–102. [PubMed: 11220366]

Murata T, Lin MI, Stan RV, Bauer PM, Yu J, Sessa WC. Genetic evidence supporting caveolae microdomain regulation of calcium entry in endothelial cells. J Biol Chem 2007;282:16631–16643. [PubMed: 17416589]

Nabi IR, Le PU. Caveolae/raft-dependent endocytosis. J Cell Biol 2003;161:673–677. [PubMed: 12771123]

Palade GE. An electron microscope study of the mitochondrial structure. J Histochem Cytochem 1953;1:188–211. [PubMed: 13069686]

Park H, Go YM, Darji R, Choi JW, Lisanti MP, Maland MC, Jo H. Caveolin-1 regulates shear stress-dependent activation of extracellular signal-regulated kinase. Am J Physiol Heart Circ Physiol 2000;278:H1285–1293. [PubMed: 10749726]

Park H, Go YM, St John PL, Maland MC, Lisanti MP, Abrahamson DR, Jo H. Plasma membrane cholesterol is a key molecule in shear stress-dependent activation of extracellular signal-regulated kinase. J Biol Chem 1998;273:32304–32311. [PubMed: 9822710]

Parton RG, Hanzal-Bayer M, Hancock JF. Biogenesis of caveolae: a structural model for caveolin-induced domain formation. J Cell Sci 2006;119:787–796. [PubMed: 16495479]

Parton RG, Simons K. The multiple faces of caveolae. Nat Rev Mol Cell Biol 2007;8:185–194. [PubMed: 17318224]

Pelkmans L, Burli T, Zerial M, Helenius A. Caveolin-stabilized membrane domains as multifunctional transport and sorting devices in endocytic membrane traffic. Cell 2004;118:767–780. [PubMed: 15369675]

Pelkmans L, Fava E, Grabner H, Hannus M, Habermann B, Krausz E, Zerial M. Genome-wide analysis of human kinases in clathrin- and caveolae/raft-mediated endocytosis. Nature 2005;436:78–86. [PubMed: 15889048]

Pelkmans L, Zerial M. Kinase-regulated quantal assemblies and kiss-and-run recycling of caveolae. Nature 2005;436:128–133. [PubMed: 16001074]

Pinaud F, Michalet X, Iyer G, Margeat E, Moore HP, Weiss S. Dynamic partitioning of a glycosyl-phosphatidylinositol-anchored protein in glycosphingolipid-rich microdomains imaged by single-quantum dot tracking. Traffic 2009;10:691–712. [PubMed: 19416475]

Prescott L, Brightman MW. The sarcolemma of Aplysia smooth muscle in freeze-fracture preparations. Tissue Cell 1976;8:241–258. [PubMed: 18631588]

Richter T, Floetenmeyer M, Ferguson C, Galea J, Goh J, Lindsay MR, Morgan GP, Marsh BJ, Parton RG. High-resolution 3D quantitative analysis of caveolar ultrastructure and caveola-cytoskeleton interactions. Traffic 2008;9:893–909. [PubMed: 18397183]

Rizzo V, Morton C, DePaola N, Schnitzer JE, Davies PF. Recruitment of endothelial caveolae into mechanotransduction pathways by flow conditioning in vitro. Am J Physiol Heart Circ Physiol 2003;285:H1720–1729. [PubMed: 12816751]

Rothberg KG, Heuser JE, Donzell WC, Ying YS, Glenney JR, Anderson RG. Caveolin, a protein component of caveolae membrane coats. Cell 1992;68:673–682. [PubMed: 1739974]

Scherer PE, Okamoto T, Chun M, Nishimoto I, Lodish HF, Lisanti MP. Identification, sequence, and expression of caveolin-2 defines a caveolin gene family. Proc Natl Acad Sci U S A 1996;93:131–135. [PubMed: 8552590]

Sedding DG, Hermsen J, Seay U, Eickelberg O, Kummer W, Schwencke C, Strasser RH, Tillmanns H, Braun-Dullaeus RC. Caveolin-1 facilitates mechanosensitive protein kinase B (Akt) signaling in vitro and in vivo. Circ Res 2005;96:635–642. [PubMed: 15731459]

NIH-PA Author Manuscript

NIH-PA Author Manuscript

NIH-PA Author Manuscript

Sens P, Turner MS. Budded membrane microdomains as tension regulators. Phys Rev E Stat Nonlin Soft Matter Phys 2006;73:031918. [PubMed: 16605569]

Sheetz MP. Cell control by membrane-cytoskeleton adhesion Nat. Rev Mol Cell Biol 2001;2:392–396.

Sorre B, Callan-Jones A, Manneville JB, Nassoy P, Joanny JF, Prost J, Goud B, Bassereau P. Curvature-driven lipid sorting needs proximity to a demixing point and is aided by proteins. Proc Natl Acad Sci USA 2009;106:5622–5626. [PubMed: 19304798]

Stan RV. Structure of caveolae. Biochim Biophys Acta 2005;1746:334–348. [PubMed: 16214243]

Tagawa A, Mezzacasa A, Hayer A, Longatti A, Pelkmans L, Helenius A. Assembly and trafficking of caveolar domains in the cell: caveolae as stable, cargo-triggered, vesicular transporters. J Cell Biol 2005;170:769–779. [PubMed: 16129785]

Vogel V, Sheetz M. Local force and geometry sensing regulate cell functions. Nat Rev Mol Cell Biol 2006;7:265–275. [PubMed: 16607289]

Woodman SE, Sotgia F, Galbiati F, Minetti C, Lisanti MP. Caveolinopathies: mutations in caveolin-3 cause four distinct autosomal dominant muscle diseases. Neurology 2004;62:538–543. [PubMed: 14981167]

Yamada E. The fine structure of the gall bladder epithelium of the mouse. J Biophys Biochem Cytol 1955;1:445–458. [PubMed: 13263332]

NIH-PA Author Manuscript

NIH-PA Author Manuscript

NIH-PA Author Manuscript

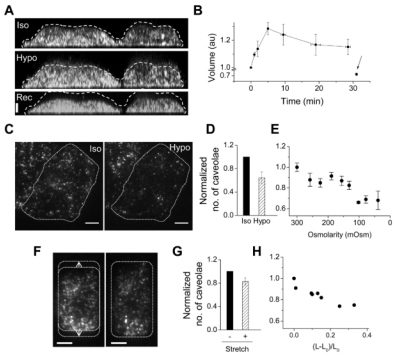

Figure 1. Mechanical Stress Induces Partial Disappearance of Caveolae

(A) YZ maximum-intensity projection of confocal stacks of Cav1-EGFP HeLa cells. Projection of 4 cells under iso-osmotic conditions (Iso), hypo-osmotic conditions (Hypo, 5 min), and 3 min after returning to iso-osmolarity (Rec). Bar = 5 μm. Dashed lines mark out the initial cell boundary.

(B) Volume of Cav1-EGFP HeLa cells tracked from (and normalized to) iso-osmotic conditions through hypo-osmotic shock (onset: t = 0 min) and upon returning to iso-osmolarity (t ~ 29 min). Arrow indicates return to iso-osmolarity. Data derived from multiple measurements (N = 5) in 3 independent experiments. Error bars represent standard deviations (SD).

(C) TIRF images of Cav1-EGFP HeLa cells under iso-osmotic conditions (Iso) and after 4 min hypo-osmotic shock (Hypo). Dotted line marks out the cell footprint. Bar = 5 μm.

(D) Change in the number of caveolae for single Cav1-EGFP HeLa cells after hypo-osmotic shock (Hypo) normalized to the number counted before hypo-osmotic shock (Iso) (N = 18). Error bars represent SD (p = 4E-11).

(E) Evolution of the loss of caveolae per cell with decreasing osmolarity. The same Cav1-EGFP HeLa cells were exposed to decreasing osmolarities during ~ 1 min for each osmolarity. From correlation analysis, the loss of caveolae is positively correlated with the decrease in external osmolarity ($r^2 = 0.85$). Error bars represent SD (N = 3).

(F) TIRF images of a Cav1-EGFP HeLa cell on the stretching device at 0% (left), and 20% stretch (right). Dotted lines mark out cell boundaries before and after stretch. Bar = 5 μm.

(G) Change in number of caveolae for single Cav1-EGFP HeLa cells after stretching (15 ± 1 %) normalized to the number counted before stretching. Data derived from multiple measurements (N = 7, p = 0.00033) in 7 independent experiments.

(H) Evolution of the number of caveolae for single Cav1-EGFP HeLa cells stretched to different lengths characterized by $(L-L_0)/L_0$ where L_0 and L are the initial and final lengths of the cell footprint in the stretching direction. Each point is measured on a single cell. The number of caveolae is found to be negatively correlated to the extent of stretch (N = 7, $r^2 = 0.85$) as measured in 7 independent experiments.

NIH-PA Author Manuscript

NIH-PA Author Manuscript

NIH-PA Author Manuscript

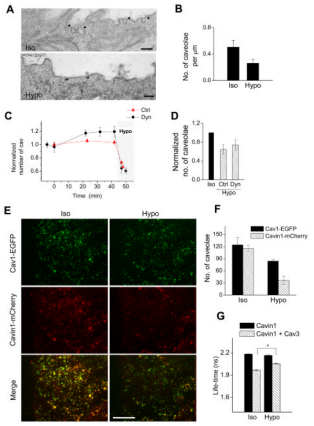

Figure 2. Caveolae Morphology and Cav1-Cavin1 Interaction is Lost Upon Hypo-Osmotic Shock

(A) Ultrathin cryosections of wt MLEC before (Iso) and 5 min after (Hypo) switch to hypo-osmotic medium examined by EM. Arrows mark out caveolae. Bar = 150 nm.

(B) Quantification of caveolae detected per μm of plasma membrane on ultrathin cryosections of wt MLEC before (Iso) and 5 min after switch to hypo-osmotic medium (Hypo) reveals a significant decrease ($p = 0.047$) in the number of caveolae after hypo-osmotic shock. Total membrane used for quantification was 76 and 67 μm for iso- and hypo-osmotic conditions, respectively, imaged from different sections of multiple randomly selected cells (> 10). Data represents mean ± SD.

(C) Time evolution of caveolae number (±SD) detected by TIRF in control (Ctrl) and dynasore treated cells (Dyn) normalized to the caveolae number before addition of dynasore ($t = -5$ min). Dynasore was added at $t = 0$ and hypo-osmotic shock was applied at $t \sim 45$ min (30 mOsm, shaded region). Error bars show SD, N = 4.

(D) Change in number of caveolae for single cells in control (Ctrl) and in dynasore treated cells (Dyn) after hypo-osmotic shock normalized to the number before shock (Iso) (N = 9). Error bars show SD ($p = 1E\text{-}4$).

(E) TIRF images of HeLa cells expressing Cavin1-mCherry and Cav1-EGFP before (Iso) and 5 min after switch to hypo-osmotic conditions (Hypo). Bar = 10 μm.

(F) Change in number of Cav1 and Cavin-1 structures per cell before and after hypo-osmotic shock of 5 min. Error bars show SD (N = 3).

(G) HeLa cells transiently expressing Cavin1-EGFP with or without Cav3-mRFP were exposed to iso-osmotic (Iso) or hypo-osmotic (Hypo) media for 15 min and analyzed by FLIM. Data represent mean EGFP fluorescence lifetime ± standard errors (SE). N = 40–70 cells; *$p < 4E\text{-}12$.

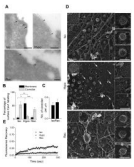

Figure 3. Caveolae Flatten out and Disassemble on Hypo-Osmotic Shock, and Reassemble on Recovering Iso-Osmolarity

(A) Immuno-EM images of ultrathin cryosections with gold-tagged Cav1 antibody of wt MLEC under iso-osmotic (Iso), hypo-osmotic (Hypo, 5 min) and recovered iso-osmotic (Rec, 5 min) conditions. Bar = 150 nm. See also Figure S2A.

(B) Percentage of gold particles found in caveolae and endosomal structures close to the plasma membrane versus those found on non-caveolar membranes (*p = 4E-3, **p=4E-2, ***p=1E-3). Total membrane used for quantification was 23, 24, and 35 μm, respectively, for iso-osmotic, hypo-osmotic, and recovered iso-osmotic conditions, imaged from different sections of multiple cells.

(C) Comparison between the number of caveolae per μm of membrane before hypo-osmotic shock (Iso) and after return to iso-osmotic medium (Rec) analyzed from ultrathin cryosections of wt MLEC using 60 μm of membrane imaged from different sections (N = 8) of multiple cells. Data represent mean ± SE (p = 1E-2).

(D) Deep-etched EM images of MLECs under iso-osmotic (Iso), hypo-osmotic (Hypo, 5 min), and recovered iso-osmotic (Rec, 5 min) conditions. Bar = 200 nm. Left insets depict representative images of clathrin-coated pits. Right images depict representative images of caveolae. Bar (insets) = 100 nm. See also Figure S2B.

(E) Fluorescence Recovery After Photobleaching (FRAP) of Cav1-EGFP in HeLa cells in iso-osmotic (Iso; N = 8), hypo-osmotic (Hypo; N = 8), and recovered iso-osmotic conditions (Rec; N = 8). Lines show fit for the curves to standard recovery equation. Hypo-osmotic shock results in a statistically higher fluorescence recovery (p = 2E-4) than in iso-osmotic conditions. Data represents mean ± SE.

NIH-PA Author Manuscript NIH-PA Author Manuscript NIH-PA Author Manuscript

NIH-PA Author Manuscript
NIH-PA Author Manuscript
NIH-PA Author Manuscript

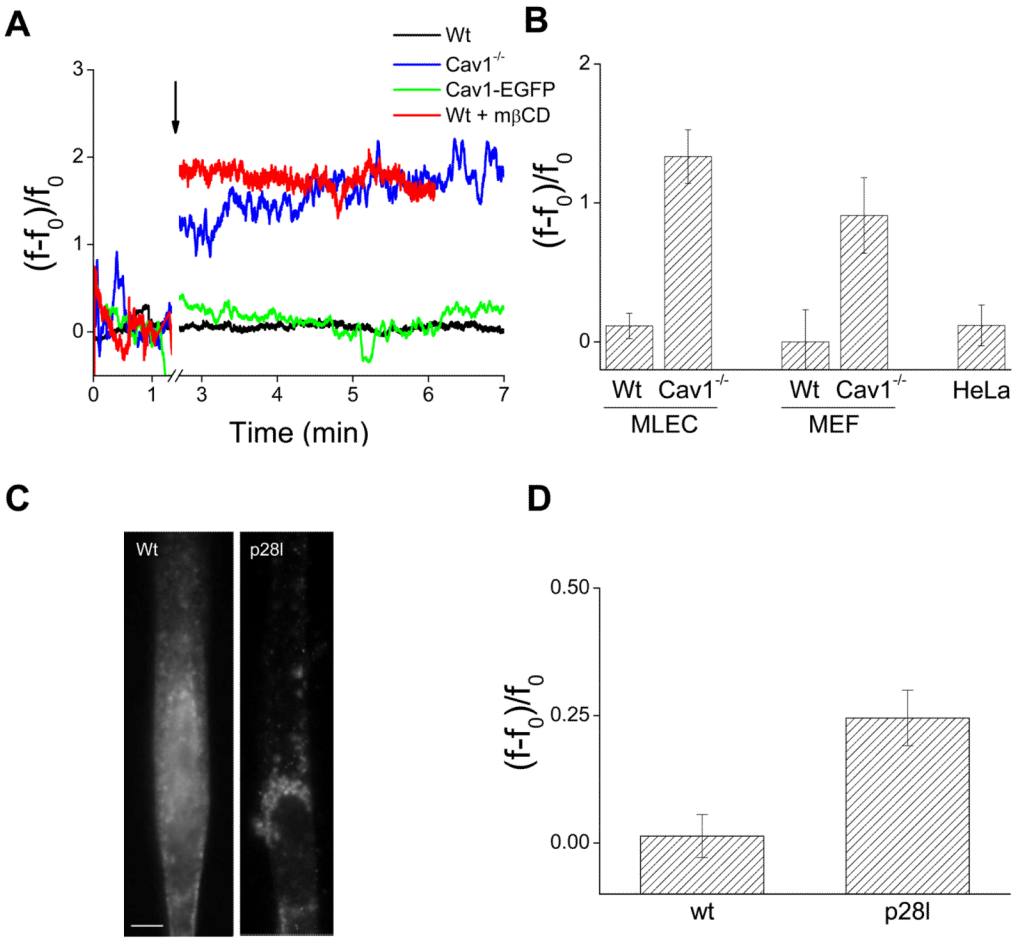

Figure 4. Caveolae Buffer the Membrane Tension Rise During Hypo-Osmotic Shock

(A) Representative force curves for tethers extracted from wt MLEC, Cav1$^{-/-}$ MLEC, Cav1$^{-/-}$ MLEC transfected with Cav1-EGFP, and wt MLEC treated with mβCD exposed to hypo-osmotic shock (150 mOsm). Hypo-osmotic shock is indicated by an arrow (break from1.34 to 2.7 min).

(B) Relative change of the mean tether force after hypo-osmotic shock (5min) for wt (N = 9), and Cav1$^{-/-}$ MLEC (N = 9, p = 0.01502), wt (N = 3) and Cav1$^{-/-}$ MEFs (N = 4, p = 8E-4) and HeLa cells (N = 4). Data represent mean ± SE. See text for details.

(C) Cav3 immunostaining in differentiated wt and Cav3-P28L human myotubes. Bar = 5 μm.

(D) Relative change of the mean tether force after hypo-osmotic shock (5 min) for wt (N = 11) and P28L myotubes (N = 12, p = 5E-8). Data represent mean ± SE.

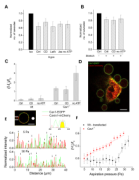

Figure 5. Membrane Tension Surge Buffering by Caveolae Flattening Occurs in an ATP and Actin Independent Process

(A) Normalized number of caveolae per cell after hypo-osmotic shock (Hypo). Reference is the number before hypo-osmotic shock (Iso) for control cells (Ctrl; N = 18). Reference is the number after the drug treatment and before hypo-osmotic shock for cytochalasin D (CD; N = 10, p = 2E-5), latrunculin A (Lat; N = 21, p = 7E-11), jasplakinolide (Jas, N = 11, p = 6E-8) treated cells, and ATP depleted cells (no ATP; N = 10, p = 2E-5). Data represent mean ± SD.

(B) Change in number of caveolae for single HeLa Cav1-EGFP cells after stretching (15 ± 1 %). Same normalization as in (A) for control cells (N = 7, p = 3E-4), and for cells treated with cytochalasin D (CD, N = 5, p = 0.01) and ATP depleted cells (no ATP, N = 5, p = 0.04). Data represent mean ± SD.

(C) Relative change of the tether force after hypo-osmotic shock (5min) for wt and $Cav1^{-/-}$ MLEC for control (Ctrl; N = 9 for wt, and for $Cav1^{-/-}$ N = 5, p = 0.015), cytochalasin D treated (CD; N = 9 for wt, and for $Cav1^{-/-}$ N = 10, p = 3E-5), and ATP depleted (no ATP; N = 6 for wt, and for $Cav1^{-/-}$ N = 5, p = 2E-4) cells. Data represent mean ± SE.

(D) Confocal image of a wt MLEC transfected with Cav1-EGFP (green) and Cavin1-mCherry (red) after incubation for 6 hrs in PMS buffer. Bar = 10 μm.

(E) Top: Confocal image of a PMS positive for Cavin1-mCherry (red) and Cav1-EGFP (green) after micropipette aspiration (white lines) and formation of a membrane tether with an optically trapped bead (white disk). Bar = 10 μm. Bottom: Line scans of cavin1-mCherry (red) and Cav1-EGFP (green) normalized intensity along the circumference of the PMS shown above for two aspiration pressures. Arrows indicate regions of co-localization.

(F) Relative change of the tether force as a function of the micropipette aspiration pressure in PMS obtained from Cav1-GFP + Cavin1-mCherry MLEC (black squares), and from $Cav1^{-/-}$ MLEC ($Cav1^{-/-}$, red triangles). Data were obtained in 8 independent experiments and represent the mean value of 60 sec measurements ± SD.

NIH-PA Author Manuscript NIH-PA Author Manuscript NIH-PA Author Manuscript

NIH-PA Author Manuscript

NIH-PA Author Manuscript

NIH-PA Author Manuscript

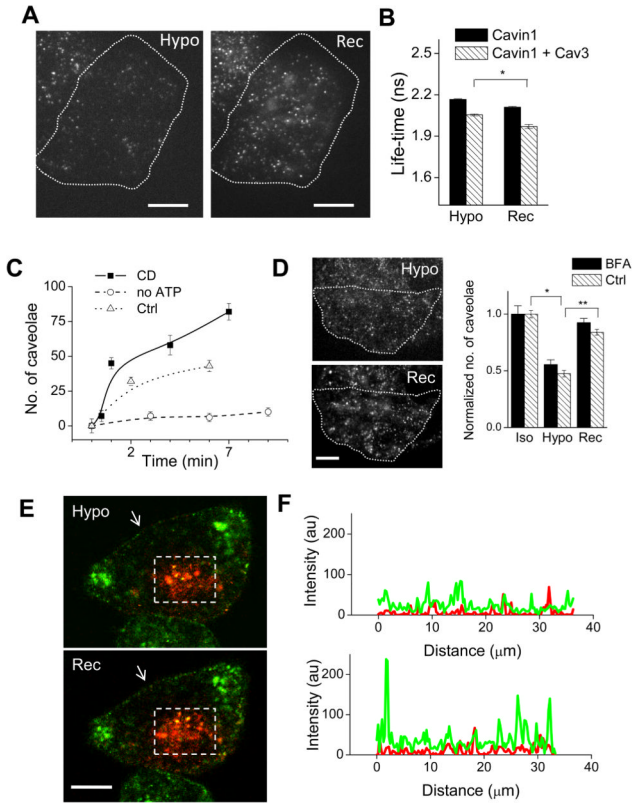

Figure 6. Caveolae Reassembly at the Plasma Membrane upon Recovering Iso-osmolarity

(A) TIRF imaging of caveolae reassembly after shifting from hypo-osmotic (Hypo) to iso-osmotic (Rec) conditions. Dotted line marks out the cell boundary. Bar = 5 μm.

(B) HeLa cells transiently expressing Cavin1-EGFP with or without Cav3-mRFP were exposed to hypo-osmotic medium (Hypo) for 15 min followed by iso-osmotic medium (Rec) for 10 min, and analyzed by FLIM. Data represent mean EGFP fluorescence lifetime ± SE (N = 40–60 cells; *p = 8E-7).

(C) After hypo-osmotic shock (15 min), cells were returned to iso-osmolarity (t = 0 min). Data represent the number of caveolae per cell for cytochalasin D treated (CD), ATP depleted (no ATP) and control cells (Ctrl). Error bars depict SD.

(D) Left panel: TIRF images show a typical BFA treated cell after 15 min hypo-osmotic shock (Hypo), and after 3 min of recovering iso-osmolarity. Bar = 10 μm. Right panel: Quantification of the number of caveolae before hypo-osmotic shock, after 15 min hypo-osmotic shock, and after 3 min of recovery to iso-osmotic conditions in BFA-treated (N = 3) and control cells (N > 10). *p = 8E-29, **p=1E-22.

(E) Cav1-Dendra2 photoconversion from green to red fluorescence at the Golgi apparatus (--- rectangle) of HeLa cells followed through hypo-osmotic shock and recovery to iso-osmotic conditions. Arrow marks out the section of the plasma membrane used for plotting intensity profiles.

(F) Intensity profiles of green (Cav1-Dendra2) and red (photoconverted Cav1-Dendra2) fluorescence at the plasma membrane before (top) and after (bottom) switch from hypo-osmotic to iso-osmotic conditions.

NIH-PA Author Manuscript

NIH-PA Author Manuscript

NIH-PA Author Manuscript

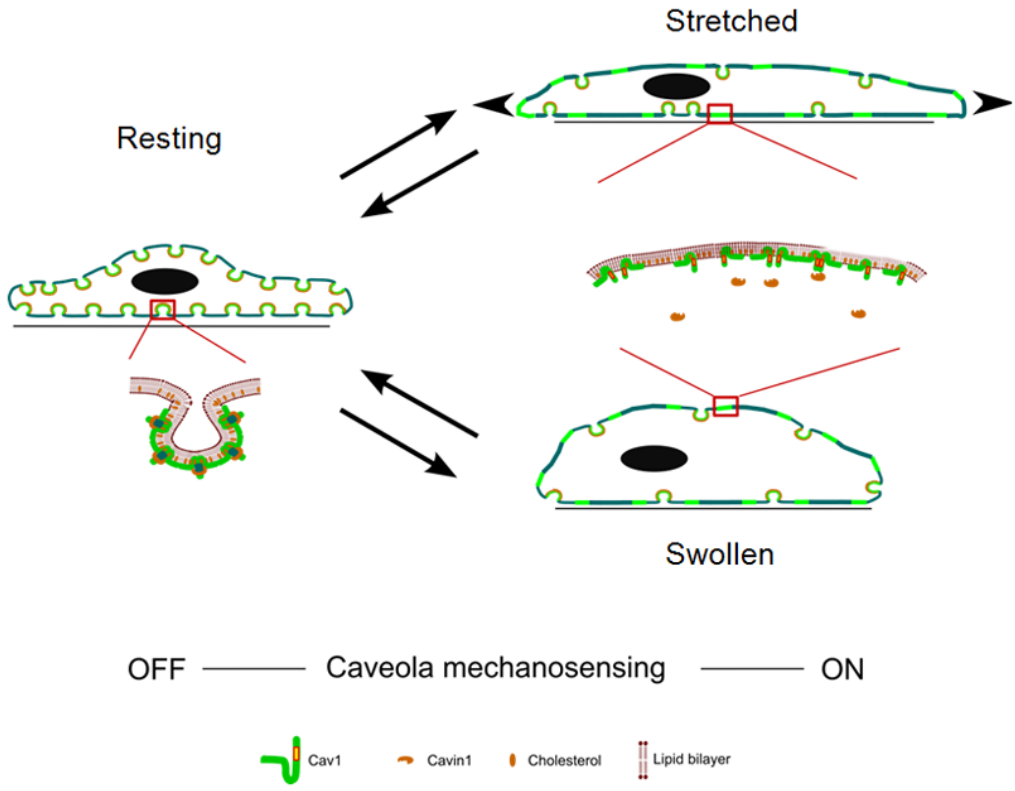

Figure 7. Cells Respond to Acute Mechanical Stresses by Rapid Disassembly and Reassembly of Caveolae

In resting conditions, caveolae present at the plasma membrane are mostly budded. Magnification shows oligomerized Cav1 and Cavin1 in the caveolar structure. Upon acute mechanical stress (hypo-osmotic shock or stretching), caveolae flatten out in the plasma membrane to provide additional membrane and buffer membrane tension. Magnification shows disassembly and diffusion of Cav1 in the plasma membrane and loss of interaction between Cav1 and Cavin1. Return to resting conditions allows the reassembly of the caveolar structure together with Cavin1 interaction. This cycle represents the primary cell response to an acute mechanical stress.